

Lattice Boltzmann Simulations of the Flow over a Hump with Flow Control

Swen Noelting¹, Michael Wessels²
Exa GmbH, Stuttgart, Germany

Anthony Keating³, Rajani Satti⁴, Yanbing Li⁵, Richard Shock⁶
Exa Corporation, Burlington, MA, 01803, USA

The wall-mounted hump test case was first presented as a benchmark problem for active flow control at the NASA sponsored workshop CFDVAL2004. For this case, both steady suction and oscillatory blowing-suction are used to control the separation and reattachment of the turbulent flow over the hump. In this paper the lattice Boltzmann method, coupled with a very large eddy simulation (VLES) turbulence model, is used to predict three cases: uncontrolled flow, controlled flow using steady suction, and controlled flow using oscillatory blowing-suction. As the lattice Boltzmann method is an inherently unsteady method it is uniquely suitable for predicting separated flows as well as flows with transient boundary conditions. We compare reattachment locations with experiments and previous CFD results. Profiles of velocity and turbulent kinetic energy in the recirculation zone and the recovery zone are also compared with experiments. Comparisons with PIV data at four phases in the oscillatory cycle are made to evaluate the accuracy of the predicted flow structures. Simulations show very good agreement with the experiments for the uncontrolled and oscillatory controlled cases, with the decrease in separation length achieved with oscillatory control accurately predicted by the lattice Boltzmann-VLES method. Simulations were found to be less accurate for the steady suction case; a reduction in recirculation length is predicted, although the reduction is smaller than observed in experiments.

Nomenclature

c_i	= Lattice Boltzmann discrete velocity vector
f_i	= Lattice Boltzmann particle distribution function
f_i^{eq}	= Lattice Boltzmann equilibrium distribution function
k	= turbulent kinetic energy
LES	= large eddy simulation
Ma	= Mach number
T	= temperature
u	= velocity
$VLES$	= very large eddy simulation
y^+	= dimensionless distance, $y u_\tau / \nu$
ε	= turbulence dissipation
τ	= lattice Boltzmann relaxation time
ρ	= density
ν	= kinematic viscosity

¹ Managing Director, Exa GmbH, AIAA Member.

² Validation Engineer, Exa GmbH

³ Manager, Aerodynamics Validation, Exa Corporation, AIAA Member

⁴ Validation Engineer, Exa Corporation, AIAA Member

⁵ Senior Validation Engineer, Exa Corporation, AIAA Member

⁶ Director, Physics Validation, Exa Corporation

I. Introduction

The effective control of flow separation promises substantial enhancement of lift for a variety of aircraft. A CFD validation workshop (CFDVAL2004) for synthetic jets and turbulent separation control was organized by NASA in 2004^{1,2,3,4} to address the currently limited understanding of this technology, both from a theoretical and a numerical modeling perspective. One of three cases in this workshop was dedicated to predicting the nominally two-dimensional flow over a wall-mounted hump. An uncontrolled baseline case was considered in addition to control by means of steady suction and zero-net-mass flux (oscillatory) blowing. Note that this case was also included in two subsequent workshops held in Europe, the 11th and 12th ERCOFTAC/IAHR Workshops on Refined Turbulence Modelling. The workshop determined that CFD with steady or unsteady Reynolds-averaged Navier-Stokes (RANS or URANS) consistently over-predicted the reattachment location⁵. Turbulence-resolving simulations, such as large-eddy simulations (LES), appeared capable of overcoming this deficiency⁶ however these methods typically result in a significant increase in computational cost.

Recently, computational fluid dynamics tools based on the lattice Boltzmann method have been applied successfully to unsteady aerodynamics problems in the aerospace industry^{7,8,9}. This method offers significant advantages over traditional RANS-based methods for the prediction of unsteady flows, due in particular to the inherently transient nature of the simulations, the very low numerical dissipation of the numerical method, the advanced turbulence modeling, and the ability to handle very complex geometries^{10,11,12,13,14}.

In the present study the Lattice-Boltzmann method is applied to the simulation of the flow over the hump. Full three-dimensional simulations of the baseline case as well as the steady suction and the oscillatory blowing cases are presented. A detailed comparison of the simulation results to the measurements is presented. The results are also compared to selected results with traditional CFD methods reported in the literature.

II. Case Description

A. Experimental Setup

The setup consisted of a wall-mounted hump model located between two glass endplates. The model had a chord of $c = 0.42\text{m}$, height of 0.0538m at its maximum thickness point, and width of 0.5842m . A diagram of the geometry is shown in Figure 1. The hump and endplates were mounted on a splitter plate and installed in an open-return atmospheric wind tunnel. Experiments were performed of the baseline case without flow control, as well as cases with steady suction and oscillatory flow control. Flow control was achieved using zero-net-mass-flux oscillatory blowing introduced from a spanwise slot located at the 65% chord station on the model, close to the location where the flow separates in the uncontrolled case. A rigid piston that was secured to the base of the plenum through a flexible membrane was used to generate the oscillatory blowing. The piston spanned the entire model to ensure two-dimensionality of the flow through the slot. Maximum slot velocities of approximately 80m/s at frequencies ranging from 60Hz to 500Hz could be achieved with this setup. The Mach number for all cases was $M = 0.1$. For the steady suction cases, the steady mass transfer momentum coefficient c_{μ} was set to 0.24% , corresponding to a mass flow rate of 0.0152 kg/s . For the unsteady blowing case the frequency was set to 138.5 Hz with a maximum outflow velocity $U_{\text{peak}} = 27\text{ m/s}$. For both cases the Reynolds number was 0.936×10^6 . The model was equipped with 165 streamwise and spanwise static pressure ports and 20 dynamic pressure ports in the separated flow region. In addition, detailed phase dependent flowfield measurements were made for the oscillatory blowing case using two-dimensional and stereoscopic particle image velocimetry (PIV).

B. Prior CFD Results

Recently, Rumsey¹⁵ performed a review of the published simulations from the CFDVAL2004 workshop and following conferences. A total of 16 groups have performed simulations of the hump case using methods including RANS, hybrid RANS/LES, LES and DNS. The initial conclusion following the workshop was that the hump case “demonstrated a failing of RANS/URANS turbulence models in general: the eddy-viscosity in the separated shear layer region was significantly underpredicted in magnitude, leading to too little mixing and hence too late a reattachment downstream”¹⁵.

Since the completion of the workshop, hybrid RANS/LES methods have gained in popularity due to their ability to resolve large-scale eddies in the separated regions of the flow, thereby reducing the reliance on the RANS turbulence model in these areas. Examples of simulations using hybrid methods were those performed by Hiller and Seitz¹⁶, Krishnan et al.¹⁷ and Saric et al.¹⁸. The hybrid methods have given mixed results. For example, the DES simulations of Saric et al.¹⁸ show good agreement for the baseline case, but when the flow control is used they see little change in the reattachment location. By far the best agreement with experiments has been obtained using LES.

As most of the eddies are resolved in LES (including those in the attached boundary layers), there is only a very small reliance on the turbulence model, but of course this comes with significant added expense. The LES of both Saric et al.¹⁸ and You et al.⁶ showed very good agreement with the experiments for both the uncontrolled and controlled cases. A summary of the reattachment locations for the various methods is shown in Table 1.

Method	Baseline	Suction	Oscillatory
Experiments	1.11 ± 0.003	0.94 ± 0.005	≈ 0.98
Typical RANS/URANS	1.24	1.10	1.22
DES ¹⁸	1.12	1.11	1.11
LES ¹⁸	1.11	0.95	1.05
LES ⁶	1.09	0.95	1.01
Present simulations	1.13	1.02	1.02

Table 1. Reattachment locations

III. Numerical Method and Computational Setup

The numerical simulations for the present study were performed with the commercial CFD code PowerFLOW. The Lattice-Boltzmann methodology underlying this code and the fluid turbulence and wall model used are described below.

A. Lattice Boltzmann Model

The present simulations have been performed using a 19 state, D3Q19, lattice Boltzmann model. The lattice Boltzmann equation is a discrete form of the Boltzmann equation, a kinetic theory based description of fluid motion. The Boltzmann equation describes the statistical distribution of particles in a fluid, macroscopic variables (such as velocity) are the direct results of the moments of this particle distribution function. By using the Chapman-Enskog expansion on the lattice Boltzmann equations, it is possible to derive the compressible Navier-Stokes equations for small Mach numbers¹⁹. In the lattice Boltzmann method used here, the collision integral in the Boltzmann equation has been approximated using the Bhatnagar-Gross-Krook²⁰ (BGK) form which leads to the lattice BGK equation:

$$f_i(\vec{x} + \vec{c}_i \Delta t, t + \Delta t) - f_i(\vec{x}, t) = C_i(\vec{x}, t) \quad (1)$$

$$C_i(\vec{x}, t) = -\frac{1}{\tau} [f_i(\vec{x}, t) - f_i^{eq}(\vec{x}, t)] \quad (2)$$

where the equilibrium distributions are approximated up to the third order as:

$$f_i^{eq} = \rho w_i \left[1 + \frac{\vec{c}_i \cdot \vec{u}}{T} + \frac{(\vec{c}_i \cdot \vec{u})^2}{2T^2} - \frac{u^2}{2T} + \frac{(\vec{c}_i \cdot \vec{u})^3}{6T^3} - \frac{\vec{c}_i \cdot \vec{u}}{2T^2} u^2 \right] \quad (3)$$

B. VLES Turbulence Modeling

Using the lattice Boltzmann equations as given above is equivalent to direct numerical simulation (DNS), where all scales of turbulence need to be resolved by the discretization of the equations²¹. At high Reynolds numbers, the resolutions requirements are so large that, even on today's supercomputers, DNS for all but the simplest geometries is not possible. Turbulence modeling is incorporated directly into the lattice Boltzmann equations by modifying the relaxation time, τ to give an extended relaxation time scale^{12,13}. The extended relaxation time is then calculated using a variant of the RNG k- ϵ equations^{15,22}. By introducing the turbulence model into the relaxation time, significantly more complex physics emerges from the RNG k- ϵ equations than from when using the Navier-Stokes equations. It can be shown that this is somewhat equivalent to a full Reynolds stress-like model²³.

The equations are modified further by incorporating a swirl correction. The swirl correction reduces eddy-viscosity in areas of high vorticity, allowing for the resolution of the unsteady large-scale vortices in regions where these

vortices can be resolved by the underlying grid. This leads to regions of the flow where turbulence is completely modeled in a RANS-like methodology (mostly near walls), and regions where turbulence is mostly resolved by the grid in an LES-like or VLES-like methodology (for example in wakes and free shear layers). Lattice Boltzmann methods are uniquely suitable for these types of simulations because they are by definition unsteady and have very low artificial diffusion. They are also computationally less demanding than traditional Navier-Stokes codes and scale extremely well on parallel hardware.

C. Wall Model

At the high Reynolds numbers typically found in aerospace applications it is often too expensive to fully-resolve the thin boundary layers found near walls (this is especially difficult when cubic grids are used). As such, wall functions are needed to model the behavior of the flow at the walls. Here we incorporate a hybrid wall function method that performs correctly at all y^+ values. When the first grid point is within the viscous sub-layer, the wall function reduces to a linear profile. When the first grid point is in the log-layer, the wall function is based on a standard log-law of the wall. The wall function is also sensitized to pressure gradients to account for the effects of favorable and adverse pressure gradients on the near-wall flow.

D. Computational Setup

For this study the complete hump geometry, including the end plates, was modeled. While this increased the size of the simulation model significantly over the two-dimensional or limited span three-dimensional models used in previous studies it removes any questions about differences caused by the different span used in experiment and simulation. Although these effects were largely neglected in previous studies the authors of the present study assumed that effects of the three-dimensionality of the flow may influence the size of the separation bubble. These effects could include blockage effects caused by the endplates or coherence effects caused by the use of artificial periodic boundary conditions in the limited span three-dimensional models.

The simulation model is shown in Figure 2 and a side view of the entire simulation domain is shown in Figure 3. The dimensions of the simulation domain are set to model the dimension of the wind tunnel. The side walls and ceiling of the tunnel are treated as inviscid walls to remove the additional cost of resolving boundary layers. An extended inflow region was used to generate the required boundary layer profile (that matched experiments) in front of the hump.

The computational grid used in the PowerFLOW simulations is shown in Figure 4. The code uses a cubic grid structure with so-called variable resolution regions to enable successive refinements of the grid structure towards areas of high gradients in the flow, or in regions where smaller cell sizes are required to resolve important geometric details (in this case the vicinity of the control slot). The regions of higher resolution can be clearly identified in Figure 3. The finest voxel size (used in the slot gap) was 0.2mm. The simulation model consisted of a total of approximately 23 million fine equivalent voxels. The simulations were run on 64 dual-processor nodes (128 total processors), and required a wall clock time of approximately 5 days for the oscillatory controlled case.

IV. Results

Results for the time-averaged reattachment locations are given in Table 1. The current simulations show good agreement for the uncontrolled case, similar in quality to both the DES and LES results. For the oscillatory controlled case the lattice Boltzmann results show a reduction in the reattachment location by ~10%, which compares very well with the experiments (~12%) and the LES (~13%). Note that previous DES studies¹⁸ showed very little change in reattachment location when oscillatory control is used. With suction control, the present simulations show a reduction of ~10%, while experimentally a reduction of ~15.3% is observed. A qualitative comparison of the fluid streamlines for the three cases is shown in Figure 5. For the uncontrolled and oscillatory controlled cases the shape (height and length) of the recirculation bubble is in very good qualitative agreement with the experiments. As indicated by the longer recirculation length, the recirculation bubble for the steady suction case is too large when compared to experiments.

Figure 6(a) shows static pressure along the centerline of the hump for the uncontrolled case. Agreement with the experiments is good. The slight overprediction of reattachment can also be observed in the static pressure plot. Centerline static pressure for the steady suction case is shown in Figure 6(b). The agreement with experiments for this case is not as good as the uncontrolled case with delayed separation and later reattachment. For the oscillatory controlled case, centerline static pressure is shown in Figure 6(c). Simulation results for this case are in excellent agreement with the experiments. Overall, the uncontrolled and oscillatory controlled cases show very good agreement with experiments for centerline static pressure and the trend between these is well predicted. With steady

suction the reattachment location is correctly moved upstream from the uncontrolled case, however the magnitude of the difference is underpredicted in the simulations.

Mean velocity profiles at $x/c = 0.8$ and $x/c = 1.2$ are shown in Figure 7. In general, there is good agreement between the simulations and experiments inside the recirculation bubble ($x/c = 0.8$). Profiles for the uncontrolled and oscillatory control at this location are in excellent agreement with experiments, in both the magnitude of the recirculating flow and the height of the bubble. For the steady suction case the agreement is not as good, the bubble is higher and stronger in the simulations than seen in the experiments. This can also be observed in the mean velocity streamlines shown in Figure 5. Downstream of reattachment, the agreement with the experiments is generally poor, primarily due to the delayed reattachment observed in the simulations.

Profiles of the turbulence kinetic energy for the three cases are shown in Figure 8 for a location within the separation bubble ($x/c = 0.8$). As the experiments only measured u and v velocity components, turbulent kinetic energy has been estimated using $k \approx 0.75 (u'u' + v'v')$. The simulation results presented here are the sum of the resolved and modeled turbulent kinetic energy, with the modeled turbulent kinetic energy being $< 10\%$ of the total indicating that the simulation is resolving most of the turbulent eddies in the separated zone. For the uncontrolled case, the agreement between the experiments and simulation is very good. The location of the peak and its magnitude is well predicted by the simulations. When oscillatory control is turned on, the peak in turbulence kinetic energy significantly increases and moves towards the wall. This trend is well captured by the simulations; however the overall magnitude of the turbulent kinetic energy is slightly overpredicted. For the steady suction case simulations significantly underpredict the turbulent kinetic energy in the bubble. This may be related to the differences in the recirculation bubble size, but because of the large difference observed between simulations and experiments there are likely to be other factors as well.

It is interesting to note that the bubble for the steady suction case in experiments is significantly more energetic than both the uncontrolled and oscillatory controlled case. This trend is not observed in the present simulations. Note that the large-eddy simulations of You et al.⁶ also found a similar discrepancy for the steady suction case: turbulent shear stress was lower in the steady suction case compared to the oscillatory controlled case. However they did find that the turbulent shear stress was larger in the steady suction case compared to the uncontrolled case which is opposite to the trend observed in the present simulations. As such, the reasons for the discrepancies in the steady suction case for the present simulations are currently unclear.

For the oscillatory flow control case PIV measurements were taken of the separated region of the flow and phase averaged. In figures 9 through 12 a comparison between the PIV measurements and the simulations are shown for spanwise vorticity at a number of locations in the phase cycle. In general, the agreement between the simulations and experiments is very good. Note that the time-averaging of the simulation data is significantly shorter than the experimental data due to the computational cost in running the simulations for very long periods of time. Simulation results were averaged over approximately 10 cycles. At the point of maximum suction the phase-averaged results show the shear-layer breaking off a large phase-averaged vortex which is then convected downstream as the cycle changes from suction to blowing. As this vortex travels downstream it breaks up at approximately the point in the cycle of maximum blowing. The “birth” of the vortex can be observed as the phase cycle changes from blowing to suction, where the shear layer begins to roll up and form the vortex.

Overall, predictions of the uncontrolled flow and the controlled flow with oscillatory blowing-suction are in good agreement with the experiments. The effect of the oscillatory control is well predicted, as are the phase-averaged flow features. The steady suction case is less well predicted, the recirculation length is too long and the turbulent kinetic energy is too low in the recirculation bubble.

V. Conclusions

A lattice Boltzmann, very large-eddy simulation method has been used to predict both the uncontrolled and controlled flow over a surface-mounted hump. Turbulent flow separation is controlled by either steady suction or by oscillatory blowing-suction. Simulations were performed with the complete wind-tunnel geometry, including the endplates. This allowed for accurate prediction of suction pressure on the top of the hump, as well as removing any questions about artificial coherency in the simulations due to the use of periodic boundary conditions. The simulations showed very good agreement for the uncontrolled case. The simulated reattachment location was slightly further downstream than found in experiments; however it was within 2% of the experiments. These results were significantly better than steady-state or unsteady RANS (which significantly overpredicted the length of the separation bubble) and close to the LES results. Centerline static pressure showed excellent agreement with experiments. Within the recirculation bubble, velocity profiles and turbulent kinetic energy profiles showed good

agreement with experiments. Velocity profiles downstream of reattachment showed relatively poor agreement due to the slightly longer recirculation bubble.

When steady suction was used to control separation, simulations showed a decrease in the reattachment length by 10%, compared to an experimental decrease of 15%. This mismatch could also be observed in the centerline static pressure. A comparison of turbulent kinetic energy in the recirculation bubble for the steady suction showed poor agreement with experiments. The agreement between experiments and simulations for the oscillatory control was significantly better. Experimentally a reduction in recirculation length of 12% was observed, while simulations predicted a 10% reduction. Centerline static pressure predicted for the oscillatory control case was in excellent agreement with experiments, as were turbulent kinetic energy and velocity profiles in the recirculation bubble. Comparisons of spanwise vorticity with phase-averaged PIV data showed that vortex formation and convection was well predicted by simulations for the oscillatory-controlled case.

Acknowledgements

The authors would like to thank Chris Rumsey (NASA Langley) and Rupesh Kotapati (Exa Corporation) for their comments on this work.

References

1. Greenblatt, D., Paschal, K. B., Yao, C.-S., Harris, J., Schaeffler, N. W., Washburn, A. E., "A Separation Control CFD Validation Test Case, Part 1: Baseline and Steady Suction," AIAA Paper 2004-2220, June-July 2004.
2. Greenblatt, D., Paschal, K. B., Yao, C.-S., Harris, J., "A Separation Control CFD Validation Test Case, Part 2: Zero Efflux Oscillatory Blowing," AIAA Paper 2005-0485, January 2005.
3. Naughton, J. W., Viken, S. A., Greenblatt, D., "Wall Shear Stress Measurements on the NASA Hump Model for CFD Validation," AIAA Paper 2004-2607, June-July 2004.
4. Seifert, A. and Pack, L. G., "Active Flow Separation Control on Wall-Mounted Hump at High Reynolds Numbers," *AIAA Journal*, Vol. 40, No. 7, July 2002.
5. Rumsey, C., and Greenblatt, D., "Parametric Study of Flow Control Over a Hump Model Using an Unsteady Reynolds-Averaged Navier-Stokes Code", NASA/TM 214897, 2007.
6. You, D., Wang, M., Moin, P., "Large-eddy simulation of flow over a wall-mounted hump with separation control," Center for Turbulence Research, Stanford, Annual Research Briefs, 2005.
7. Satti, R., Li, Y., Shock, R., Noelting, S., "Simulation of Flow over a 3-Element Airfoil Using a Lattice-Boltzmann Method" AIAA Paper 2008-549, January 2008.
8. Satti, R., Li, Y., Shock, R., Noelting, S., "Unsteady Flow Simulation of a High Lift Trapezoidal Wing Using Lattice Boltzmann Method", AIAA Paper 2008-4145, June 2008.
9. Keating, A., Beedy, J. and Shock, R., "Lattice Boltzmann Simulations of the DLR-F4, DLR-F6 and Variants", AIAA Paper 2008-749, January 2008.
10. Chen, H., Teixeira, C. and Molvig, K., "Digital Physics Approach to Computational Fluid Dynamics, Some Basic Theoretical Features," *Intl. J. Mod. Phys. C*, Vol. 8, No. 4, 1997, pp. 675.
11. Chen, H., Teixeira, C., Molvig, K., "Realization of Fluid Boundary Conditions via Discrete Boltzmann Dynamics," *Intl. J. Mod. Phys. C*, Vol. 9, No.8, 1998, pp. 1281.
12. Chen, H., Kandasamy, S., Orszag, S., Shock, R., Succi, S. and Yakhot, V., "Extended Boltzmann Kinetic Equation for Turbulent Flows", *Science*, Vol. 301, 2003, pp. 633-636
13. Chen, H., Orszag, S., Staroselsky, I. and Succi, S., "Expanded Analogy between Boltzmann Kinetic Theory of Fluid and Turbulence", *J. Fluid Mech.*, Vol. 519, 2004, pp. 307-314.
14. Yakhot, V., Orszag, S., Thangam, S., Gatski, T. and Speziale, C., "Development of turbulence models for shear flows by a double expansion technique," *Phys. Fluids A*, Vol. 4, No. 7, 1992, pp. 1510-1520.
15. Rumsey, C., "Successes and Challenges for Flow Control Simulations," AIAA Paper 2008-4311, June 2008.
16. Hiller, S.J. and Seitz, P.A. "The Interaction Between a Fluidic Actuator and Main Flow Using SAS Turbulence Modeling," AIAA Paper 2006-3678, June 2006.
17. Krishnan, V., Squires, K.D. and Forsythe, J.R., "Prediction of Separated Flow Characteristics over a Hump," *AIAA Journal*, Vol 44, No. 2, 2006, pp. 252-262.

18. Saric, S., Jakirlic, S., Djugum, A. and Tropea, C., "Computational Analysis of a Locally Forced Flow over a Wall-Mounted Hump at High-Re Number," *Int. J. Heat and Fluid Flow*, Vol. 27, No. 4, 2006, pp. 707-720.
19. Chen, H., Chen, S. and Matthaeus, W., "Recovery of the Navier-Stokes Equations Using a Lattice-gas Boltzmann Method," *Phys. Rev. A*, Vol 45, 1992, pp. 5339-5342.
20. Bhatnagar, P., Gross, E. and Krook, M., "A Model for Collision Processes in Gases. I. Small Amplitude Processes in Charge and Neutral One-component System," *Phys. Rev.*, Vol. 94, 1954, pp. 511-525.
21. Li, Y., Shock, R., Zhang, R. and Chen, H., "Numerical Study of Flow Past an Impulsively Started Cylinder by Lattice Boltzmann Method," *J. Fluid Mech.*, Vol. 519, 2004, pp. 273-300.
22. Yakhot, V. and Orszag, S.A., "Renormalization Group Analysis of Turbulence. I. Basic Theory," *J. Sci. Comput.*, Vol. 1, No. 2, 1986, pp. 3-51.
23. Orszag, S.A., personal communication, 2008.

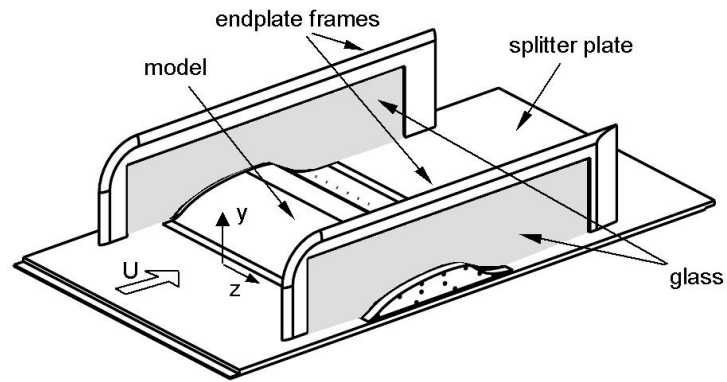


Figure 1: Experimental Setup

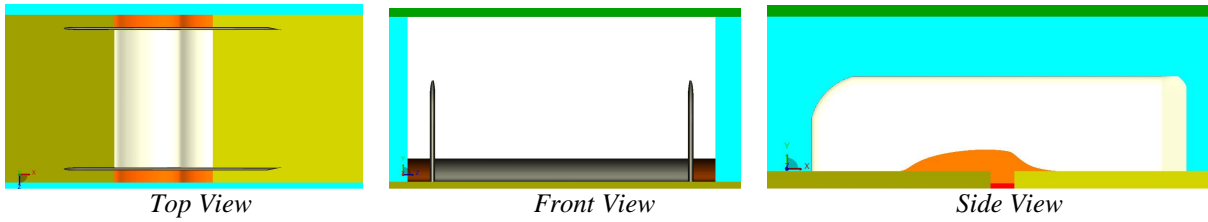


Figure 2: Simulation Model

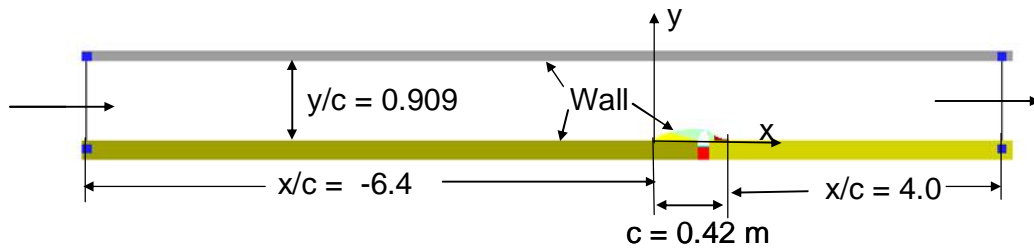


Figure 3: Simulation Domain

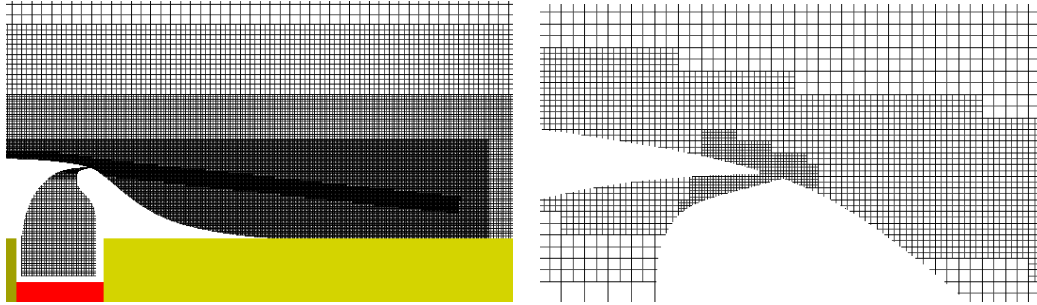


Figure 4: Computational Lattice

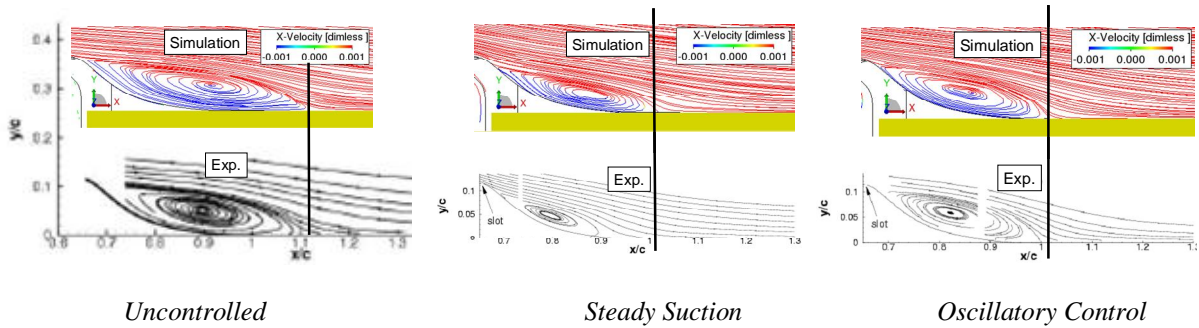
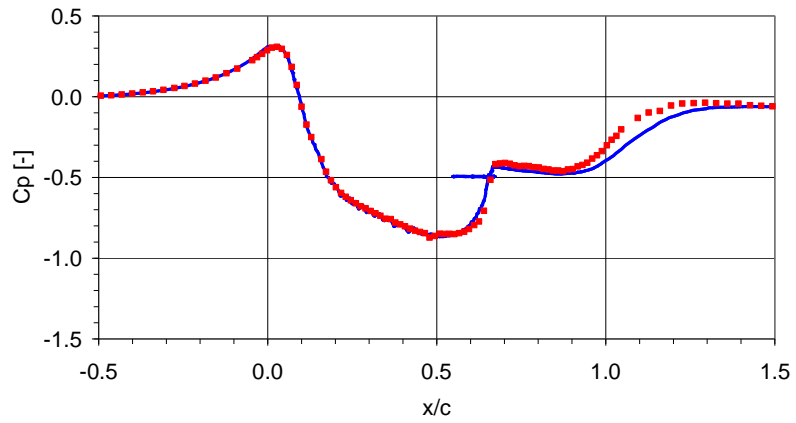
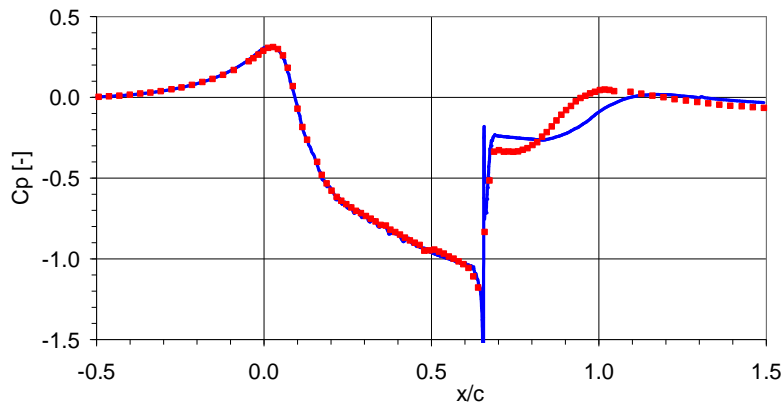


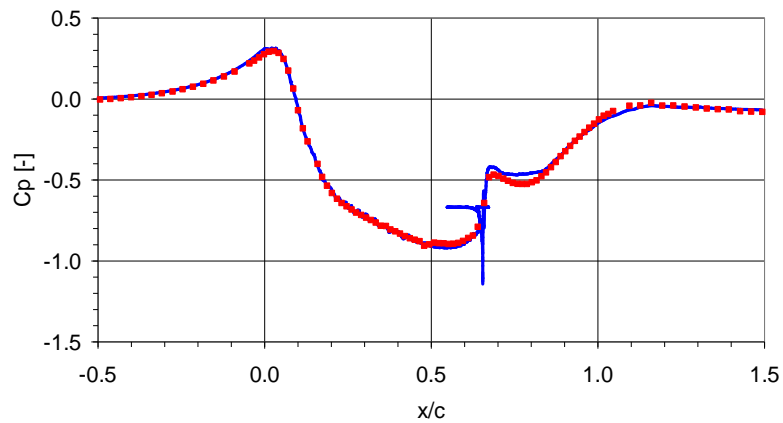
Figure 5: Resultant fluid streamlines and reattachment locations.



(a) Uncontrolled case

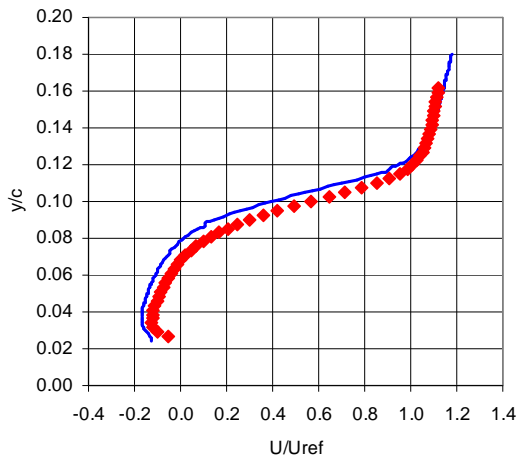


(b) Steady suction case

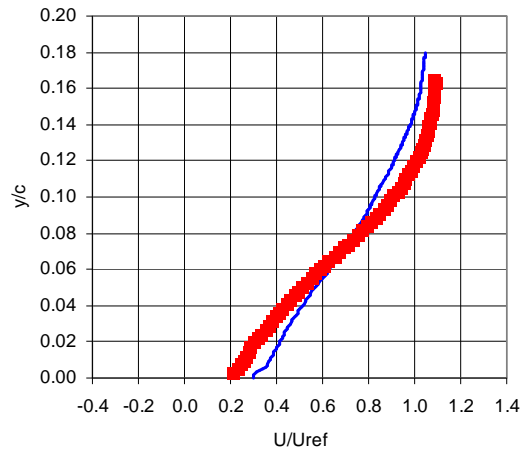


(c) Oscillatory control case

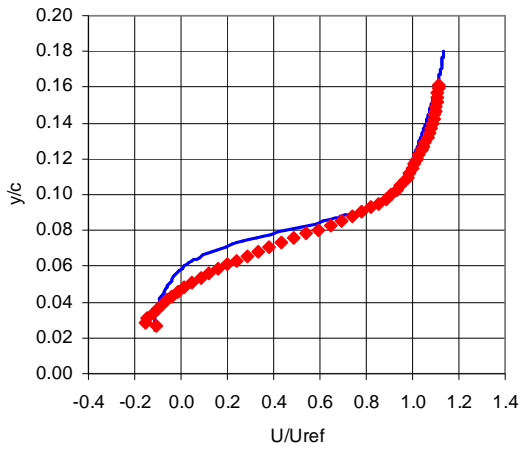
Figure 6: Surface c_p . Lines are simulations, points are experiments.



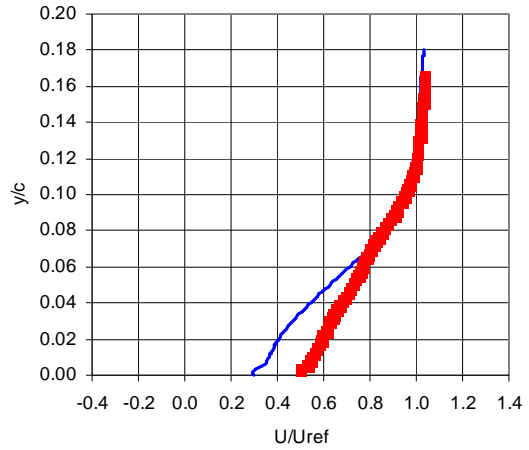
(a) Uncontrolled case, $x/c = 0.8$



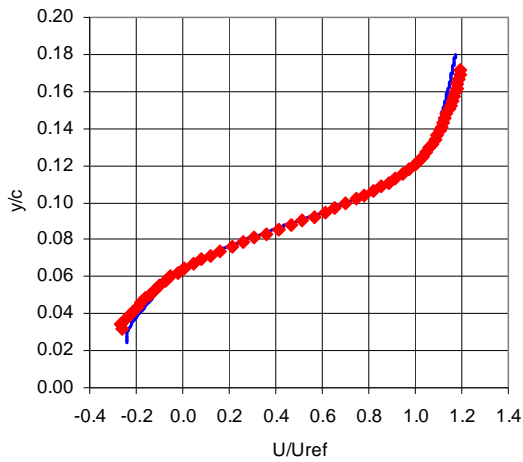
(b) Uncontrolled case, $x/c = 1.2$



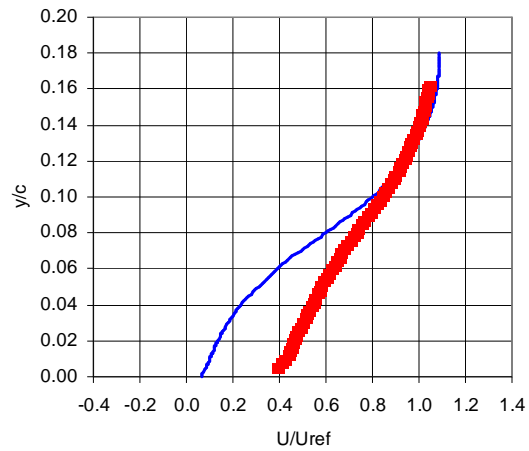
(c) Steady suction, $x/c = 0.8$



(d) Steady suction, $x/c = 1.2$



(e) Oscillatory control, $x/c = 0.8$



(f) Oscillatory control, $x/c = 1.2$

Figure 7. Mean velocity profiles. Lines are simulation, points are experiments.

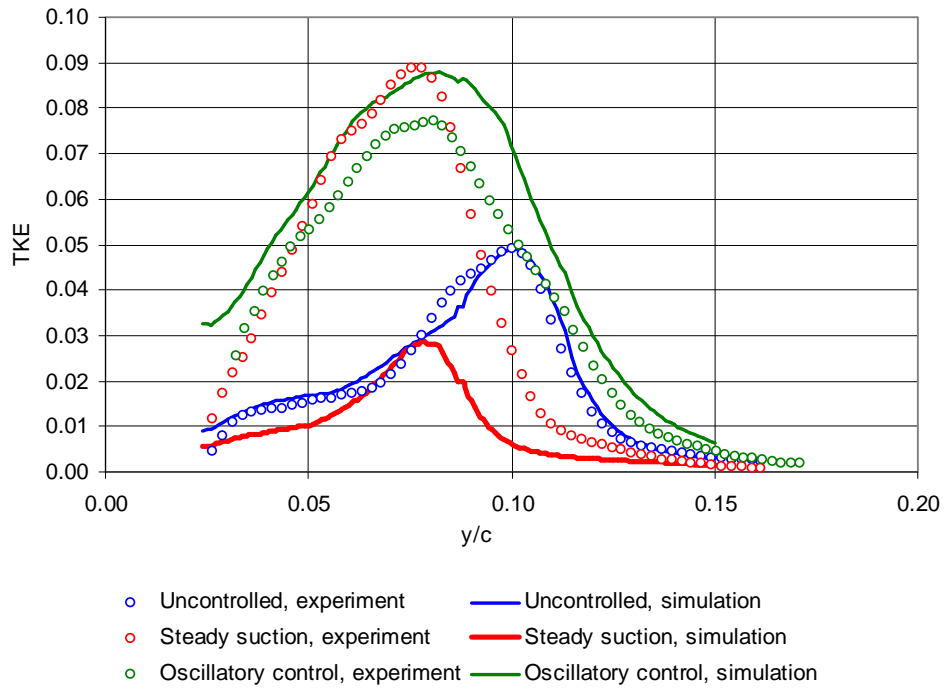


Figure 8. Turbulence kinetic energy profiles at $x/c = 0.8$

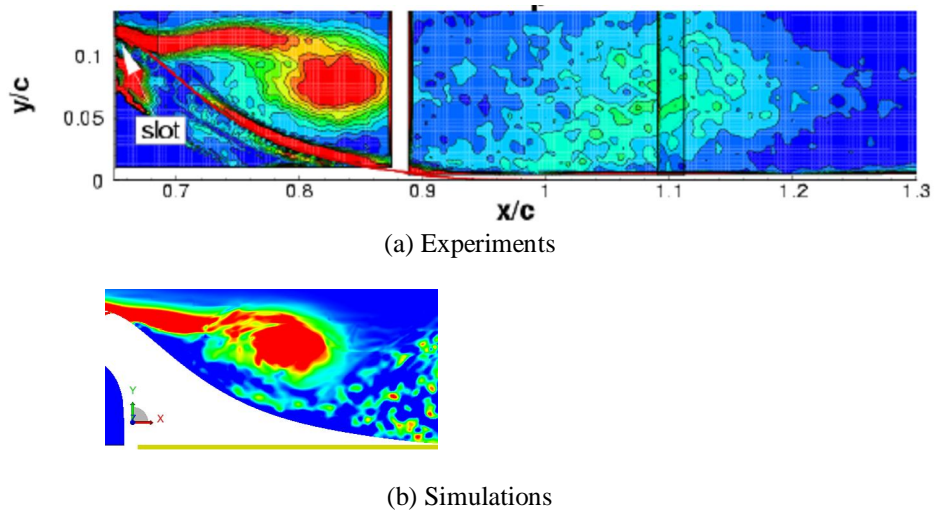
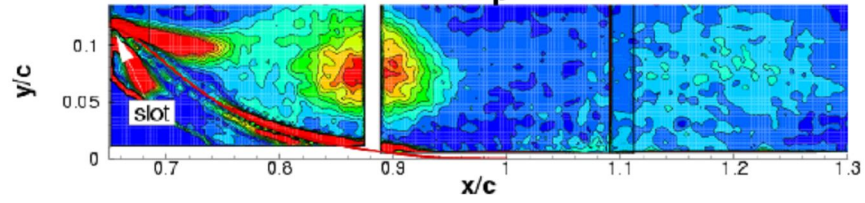
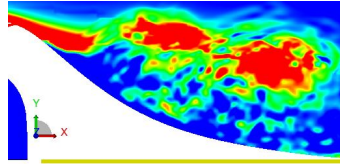


Figure 9. Phase-averaged spanwise vorticity at maximum suction phase location

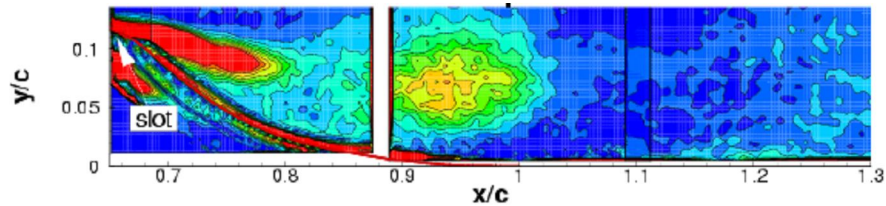


(a) Experiments

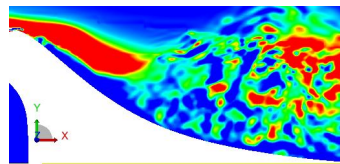


(b) Simulations

Figure 10. Phase-averaged spanwise vorticity at suction to blowing phase location

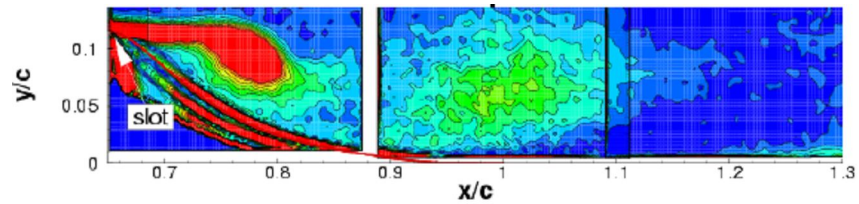


(a) Experiments

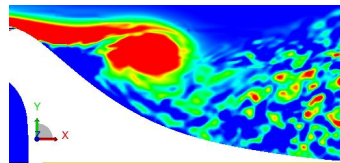


(b) Simulations

Figure 11. Phase-averaged spanwise vorticity at maximum blowing phase location



(a) Experiments



(b) Simulations

Figure 12. Phase-averaged spanwise vorticity at blowing to suction phase location